Water Structure at the Air−Aqueous Interface of Divalent Cation and Nitrate Solutions†

Man Xu, Rick Spinney, and Heather C. Allen*

Department of Chemistry, The Ohio State University, 100 West 18th Avenue, Columbus, Ohio 43210

Received: July 24, 2008; Revised Manuscript Received: December 4, 2008

The water surface structure of aqueous magnesium, calcium, and strontium nitrate solutions with six to seven water molecules on average solvating each ion was investigated using vibrational sum frequency generation (VSFG) spectroscopy. Raman (polarized) and infrared spectroscopies were used for understanding solvation effects. Infrared reflection spectra were analyzed to further understand the VSFG data. The VSFG spectral changes indicate that the divalent countercation species play a key role in the surface perturbation of the water. In addition, the data show that the solvated ions, and possibly their ion pairs, approach the aqueous surface. The identity of the divalent cation may cause a difference in the concentration gradient near the surface, thereby increasing the VSFG-active region, which then indicates an increase in the interfacial depth. The interface becomes thickened with $Mg^{2+} < Ca^{2+} < Sr^{2+}$. The free OH orientation measured from the surface normal from the salt solutions changes from 33 (from neat water) to ∼60°.

Introduction

The ubiquitous existence of water in the environment and biological systems makes understanding the water structure at interfaces of great interest. Also of interest is understanding the surface propensity of ions and molecules at the air−aqueous interface and the structure and dynamics of mediating water molecules. Understanding the behavior of both the solute and solvent are critically important to further deconvolute more complex phenomena such as those occurring in atmospheric aerosols, aqueous geochemical systems, and biological systems. Yet, understanding water and its hydrogen-bonding character, in the bulk and at its air interface, is in itself complex.

At the air−aqueous interface, hydrogen bonding between water molecules is somewhat distorted due to the interfacial environment, hydrophobic air on one side, and hydrophilic bulk water on the other. Second-order optical spectroscopy experiments, second harmonic generation,[1] and vibrational sum frequency generation[2,3] indicate that, on average, the surface water molecules have their dipoles somewhat parallel to the interface and pointed slightly toward the bulk solution. Additionally, about 20% of surface water molecules have a dangling OH.[2] This free OH is relatively uncoupled from the rest of the water molecule on which it resides, although the nonfree OH of this water molecule is coupled to surrounding water through a dynamic hydrogen-bonding network.

Recently, studies of the water structure at the air−aqueous inorganic−ion interface have revealed details about aqueous surfaces and the surface preponderance of highly water soluble ions.[4−8] The long-standing view of the air−aqueous interface of inorganic salt solutions is that these interfaces are devoid of ions.[9,10] This commonly accepted view was based on macroscopic surface tension data and the Gibbs adsorption equation. An increase of the surface tension from that of water was interpreted as a surface depletion of ions. However, this commonly held simplistic interpretation is only sometimes correct.

The alternative interpretation is that there is a net depletion of ions in the interfacial region, and this depletion can take form over many water layers until the ion concentration is constant, that is, in the bulk solution. It is now believed, on the basis of experimental[4,11−16] and theoretical[12,14,17−20] work, that large polarizable halide anions (bromide and iodide) reside in the surface region with their counter monovalent cation residing, on average, below the anion. At the depth of the cation preponderance, the anion concentration is predicted to be somewhat depleted; then, both the cation and anion approach a constant bulk concentration. The region from the surface topmost water layer to the depth of this constant bulk concentration is defined as the interface. Gradients of ion concentration can change direction and provide structure in the surface and subsurface water regions, the air−aqueous interface.

In addition to large, polarizable halide anions possessing surface activity, ions such as SCN^-,[14] N_3^-,[16] and NO_3^- [21−23] also have been shown to exhibit a propensity for the air−aqueous interface. For NO_3^-,[21−24] theorists are somewhat in agreement that the nitrate anion approaches the interface; however, there is not a surface excess beyond what is found in the bulk solution. Importantly, predicted theoretically, nitrate is not depleted from the air−aqueous interface. The recent MD simulations[21,23,24] incorporate ion polarizability for NO_3^- with and without a monovalent counterion.

The theoretical supposition that nitrate ions can exist in the first few layers of the air−aqueous interface is intriguing. We have recently completed a VSFG study in which we observe the nitrate symmetric stretch vibration, thereby revealing that, in fact, nitration anions are directly observable in the interface, in the surface, or in the subsurface region.[25] Additionally, Shultz and co-workers,[7] using VSFG, showed changes to the hydrogen-bonding network and the free OH at the air−aqueous interface of a monovalent cation−nitrate salt solution, aqueous sodium nitrate. Clearly, these experimental studies reveal that nitrate is present and causes perturbation of the interfacial water.[7,25]

Past theoretical and experimental studies investigated monovalent cations with monovalent anions and, in some cases, divalent anions at the air−aqueous interface. There are relatively few VSFG studies of divalent cations[26] and none that have

† Part of the special section "Aqueous Solutions and Their Interfaces".

* To whom correspondence should be addressed. E-mail: allen@chemistry.ohio-state.edu.

10.1021/jp806565a CCC: $40.75
Published on Web 02/24/2009

interrogated interfacial water structure of aqueous divalent cations with the nitrate anion. Divalent cations are of particular interest because of their high charge. Surface charge density then becomes important in aqueous ionic systems. Mg^{2+} has a high surface charge density relative to Ca^{2+} and Sr^2, which are also in the alkali earth metal category of the periodic table. As the size of the divalent cation increases, the surface charge density decreases. This has consequences in the bulk solution, as well as at the air−aqueous interface, as we show in this paper.

Nitrate is unique among monovalent anions. Relative to the recently studied surface-active bromide and iodide anions, which are considered spherical in aqueous solution, nitrate is planar with a D_{3h} symmetry. However, the fact that the nitrate symmetric stretch has been detected with VSFG[25] points to the distortion of the planar structure in the interface since the symmetric stretch of the D_{3h} symmetry would not be VSFG-active (arising from the lack of IR activity; VSFG-active modes must be both IR- and Raman-active).[3,5,27,28]

In the work presented here, we show a series of VSFG studies designed to better understand water at its air−aqueous interface and the role of divalent cations and the nitrate anion at the air−aqueous salt interface. We recently directly studied nitrate ions at the aqueous interface[25] and divalent metal−nitrate ion pairing in the bulk.[29] These studies suggested that the presence of these ions and the formation of ion pairs may have considerable effects on the hydrogen-bonded structure of water at the air−aqueous interface. The work presented here further explores the structure of the air−aqueous interface of Mg^{2+}, Ca^{2+}, and Sr^{2+} nitrate solutions. Our approach is one that continues to be refined in its rigor to fully understand the VSFG data inclusive of developing additional analysis methods incorporating reflection infrared absorption spectral analysis.

Vibrational sum frequency generation spectroscopy continues to emerge as a powerful technique for investigating the interfacial structure of liquids and solids.[3−5,8,28,30,31] VSFG is used as the primary experimental tool in this study. Details of VSFG theory are found in the literature.[5,27,28,30] Briefly, it is an inherently interface-specific technique that provides molecular-level spectroscopic information. In addition to infrared and Raman activity being a requirement for VSFG activity, VSFG spectra obtained from interfaces arises from lack of inversion symmetry and molecular and macroscopic noncentrosymmetry. Therefore, VSFG can provide surface and subsurface information. The depth of penetration of the incident light used in the VSFG experiment is on the order of its wavelength. The coherence length of the incident infrared and visible beams further shortens the VSFG-available probe depth. However, the VSFG signal only arises from the noncentrosymmetric region of that depth. This selection rule is critical to the understanding of VSFG data and is exploited in this work to evaluate the interfacial depth, that is, regions of ion concentration gradients.

Experimental Section

VSFG Instrumentation. The VSFG spectra were acquired on a scanning VSFG system. This scanning VSFG system uses a pulsed Nd:YAG laser (29 ps pulse duration and 10 Hz repetition rate, ESKPLA, PL 2143A/SS) that pumps a KTP-KTA-based optical parametric generator/amplifier (LaserVision). The mid-infrared beam generated is tunable from 2500 to 4000 cm^{-1} with a bandwidth of 4−8 cm^{-1} and energy of 200−500 μJ/pulse at the sample surface, depending on the spectral region. The 532 nm visible beam is ~550 μJ/pulse at the sample surface. The input angles are set to 45 and 53° from the surface normal for the 532 nm and infrared beams, respectively. A cooled charge-coupled device (CCD) camera (Andor Technology, DV887ECS-BV) is utilized to collect the VSFG signal. An iris, a Schott glass filter (BG 25, CVI Laser), a short pass filter (SPF500, CVI laser), and two holographic notch plus filters (Kaiser Optical System, Inc.) are used before the CCD camera to block the 532 nm scattered light. Polarization combinations, ssp and ppp, were obtained; ssp refers to the VSFG, visible, and infrared beams, in that order. The s-polarization is light linearly polarized perpendicular to the incident plane, whereas p-polarization is light linearly polarized in the plane of incidence. VSFG data points as plotted were collected every 10 cm^{-1} in the 2800−3680 cm^{-1} region, every 5 cm^{-1} in the 3680−3740 cm^{-1} region, and every 10 cm^{-1} in the 3740−3800 cm^{-1} region. The exposure time for each data point was 15 s (150 pulses per data point). All VSFG spectra presented in this paper are plots of the sum frequency intensity versus the incident infrared frequency and are the average of three replicate spectra. Error bars are the standard deviation of the data. The VSFG spectra were normalized to IR profiles detected in real time with VSFG and were then normalized to the Fresnel factors (details of this normalization process are found in the Supporting Information). To ensure the stability of the VSFG system and to confirm the reproducibility of the spectra, VSFG spectra of neat water were also obtained at the beginning and the end of daily experiments.

Raman Instrumentation. Raman spectra, unpolarized and polarized (parallel and perpendicular), were obtained. Unpolarized Raman spectra were acquired by passing a beam of unpolarized 532 nm light from a continuous wave laser (Spectra-Physics, Millennia II) onto the sample using a 5 mm focusing fiber optic Raman probe (InPhotonics, RPS532/12-10). The Raman scatter, collected by a second fiber optic, exited through a fiber optic imaging coupler (Acton Research, FC-446-030) and was focused onto the entrance slit of a 500 mm monochromator (Acton Research, SpectroPro SP-500). The scatter was dispersed by a 600 groove/mm grating blazed at 1 μm and collected on a liquid-nitrogen-cooled CCD camera (Roper Scientific, LN400EB, 1340 × 400 pixel array, back-illuminated and deep depletion CCD). The power of the 532 nm beam for sample illumination was ~100 mW, and the monochromator entrance slit width was set to 50 μm. To obtain the polarized Raman spectra, a 90° configuration for the incoming laser beam and detection was used. Linear polarizing films (Edmund Optics) were placed before and after the sample. The incoming 532 nm beam from the Raman probe was polarized before illuminating the sample. After the sample, the parallel or the perpendicular component of the Raman scattered light was focused onto the entrance slit of the monochromator using a BK7 lens (focal length of 75 mm). A long-pass 535 nm filter (Omega Optical, Custom) was placed in the light path before the monochromator to remove the 532 nm Rayleigh scattering. Unpolarized spectra were collected with an exposure time of 50 s, while polarized spectra were collected with an exposure time of 5 min. Before data collection, the monochromator was calibrated using the 435.833 nm Hg line of a fluorescent light. The calibration of the wavenumber position was completed after obtaining and comparing Raman spectra of crystalline naphthalene.

Infrared Instrumentation. Two different types of infrared experiments were performed, infrared reflection absorption spectroscopy (IRRAS) and attenuated total reflection Fourier transform infrared (ATR-FTIR).

For the IRRAS experiments, an infrared microscope (PerkinElmer Spectrum Spotlight 300 FT-IR microscope) was used. Spectra were collected by using the reflectance sampling mode, where the infrared beam was incident on the air−aqueous

TABLE 1: Concentrations of the Nitrate Aqueous Solutions

molality (m)	salt mole fraction (x)	molarity (M) $Mg(NO_3)_2$	$Ca(NO_3)_2$	$Sr(NO_3)_2$
0.50	0.0089	0.47	0.46	0.49
2.6	0.045	1.9	2.0	2.3
3.3	0.056	2.2	2.3	2.7

interfaces of the solutions, and the reflected beam was analyzed. Both the incident and the reflected angles were 27° to the surface normal. The IR microscope aperture was set to 100 × 100, the spectral resolution was 2.00 cm^{-1}, and each spectrum was averaged over 512 scans. A Kramers−Kronig transformation (PerkinElmer software, Spectrum, version 6.2.0) was performed on the IRRAS spectra to reveal the real refractive index and the imaginary contributions from the reflectance spectrum.

For the ATR-FTIR experiments, a Thermo Nicolet Fourier transform infrared (FTIR) spectrometer (Thermo Electron Corporation, Avatar 370) was employed. The ATR-FTIR experiments were conducted using a ZnSe crystal mounted on a 45° single-bounce ATR accessory (Thermo Electron Corporation, Smart SpeculATR). Spectra were collected with a spectral resolution of 4 cm^{-1} and were averaged over 128 scans.

IRRAS experiments were performed to refine our VSFG analysis methods by comparing the VSFG data to air−aqueous interfacial reflected IR data. ATR-FTIR instead of transmission FTIR was used as a bulk probe in the present work since it proved difficult to reproducibly obtain transmission spectra with path lengths small enough to avoid detector saturation. Note that the IR penetration depth for ATR-FTIR is on the order of the wavelength of the incident light, and therefore, the IR absorption is dominated by the bulk contribution. This is also true for the IRRAS experiments. The obtained ATR-FTIR spectra are referred as IR spectra in this paper.

All spectroscopy experiments were performed at room temperature (24 ± 2 °C).

Chemicals. Nitrate salts, $Mg(NO_3)_2 \cdot 6H_2O$ (certified ACS, 98.0−102.0%), $Ca(NO_3)_2 \cdot 4H_2O$ (certified ACS, 99.0−103.0%), $Sr(NO_3)_2$ (certified ACS, 99.0%), were purchased from Fisher Scientific. The aqueous solutions were made using Nanopure water with a resistivity of 18.0−18.3 MΩ cm and filtered, typically three to six times, using a carbon filter (Whatman Carbon-Cap 150) to remove organic impurities. Raman spectra were utilized to generate a calibration curve, and the concentrations after filtration were determined from the calibration curve. VSFG spectra in the 2800 to 3000 cm^{-1} region were obtained to check for organic impurities in the salt solutions. Aqueous solutions of 2.6 and 3.3 m (molality) were studied in the present work; 2.6 m corresponds to 0.045 x (mole fraction), and 3.3 m corresponds to 0.056 x for all salts. Table 1 shows the concentration unit conversions of m, x, and M (molarity).

Results and Discussion

The VSFG spectra of the air−neat water interface and the Raman and IR spectra of bulk water in the OH stretching region (3000−3800 cm^{-1}) are shown in Figure 1. The broad continuum spanning from ∼3000 to ∼3600 cm^{-1} of the VSFG (Figure 1a−b), Raman (Figure 1c−d), and IR (Figure 1e) spectra is assigned to the OH stretching modes of hydrogen-bonded water molecules. Though the precise assignment of the 3000−3600 cm^{-1} continuum remains controversial,[3,8,31,32] there is a general relationship between the frequency of the OH stretch and the length and strength of the hydrogen bonds.[33] The lower frequencies beginning at ∼3000 cm^{-1} arise from the OH stretching modes of strongly hydrogen-bonded water molecules within the hydrogen-bonding network. The observed resonances at higher frequencies arise from less strongly hydrogen-bonded water molecules. Intermolecular coupling and, moreover, collective modes also play a major role in the observed frequencies. Not part of the continuum in the VSFG spectrum shown in Figure 1a,b is a narrow peak at 3700 cm^{-1}, which is assigned to the dangling OH (free OH) stretch of water molecules that span across the air−water interface with one uncoupled OH bond directed into the gas phase and the other interacting through hydrogen bonding with the liquid phase.

The VSFG spectrum shown in Figure 1a was normalized to the real-time IR profile. However, the VSFG intensity is proportional to the intensities of the incident beams and the square of the absolute value of the effective sum frequency susceptibility.[30,34] The latter term is associated with the Fresnel factors. Figure 1b shows the resulting VSFG spectrum of neat water after normalization to the IR intensities (the intensity of visible light is constant) and the Fresnel factors. (Detailed calculations of the Fresnel factors are found in the Supporting Information.) As shown in Figure 1a,b, small differences in the hydrogen-bonded OH stretching region are observed when using different normalization methods.

In addition to unpolarized Raman (Figure 1c), polarized Raman experiments were performed. The obtained polarized Raman spectra of neat water are shown in Figure 1d, where the solid line refers to the parallel-polarized Raman spectrum (Raman scattering polarized in the same plane as the incident light), and the dashed line refers to the perpendicular-polarized Raman spectrum (Raman scattering polarized perpendicular to the plane of polarization of the incident light). The parallel-polarized instead of the unpolarized Raman spectra are employed later for the comparison between the bulk Raman and IR intensities and the interfacial ssp-polarized VSFG intensities.

Figure 1e shows the ATR-FTIR spectrum of the bulk water. Figure 1f provides the spectrum of the imaginary refractive index, k, obtained through IRRAS and the Kramers−Kronig transformation. The complex reflectance spectrum from the IRRAS experiment is mathematically decomposed into two separate spectra that are related by the Kramers−Kronig relationship, the imaginary refractive index (k, also called extinction coefficient) and the real refractive index (n) spectra. According to the Beer−Lambert law, k is proportional to the absorbance. This is consistent with the similarity between the k spectrum of water (Figure 1f) and the IR spectrum from transmission FTIR (spectrum not shown here).

To understand the hydrogen-bonding network of the bulk water after addition of nitrate salts, a series of Raman and IR spectra were acquired for 0.045 and 0.056 x $Mg(NO_3)_2$, $Ca(NO_3)_2$, and $Sr(NO_3)_2$ aqueous solutions. The unpolarized Raman spectra of these solutions are shown in Figure 2a,b, and the ATR-FTIR spectra are shown in Figure 2c,d. With the addition of nitrate salts to water, the Raman bulk spectra clearly reveal a decrease in the low-frequency side (∼3200 cm^{-1}) of the hydrogen-bonded continuum and a small intensity increase in the high-frequency side (∼3400 cm^{-1}) of the continuum. The low-frequency and high-frequency sides of the spectrum are referred to as the 3200 and 3400 cm^{-1} bands in this paper, respectively. The ATR-FTIR bulk spectra (Figure 2c,d) show a decrease and narrowing of the 3200 cm^{-1} band and no significant enhancement of the 3400 cm^{-1} band, although broadened to higher wavenumber.

Figure 3 shows the polarized Raman spectra (parallel and perpendicular) of nitrate aqueous solutions with a concentration

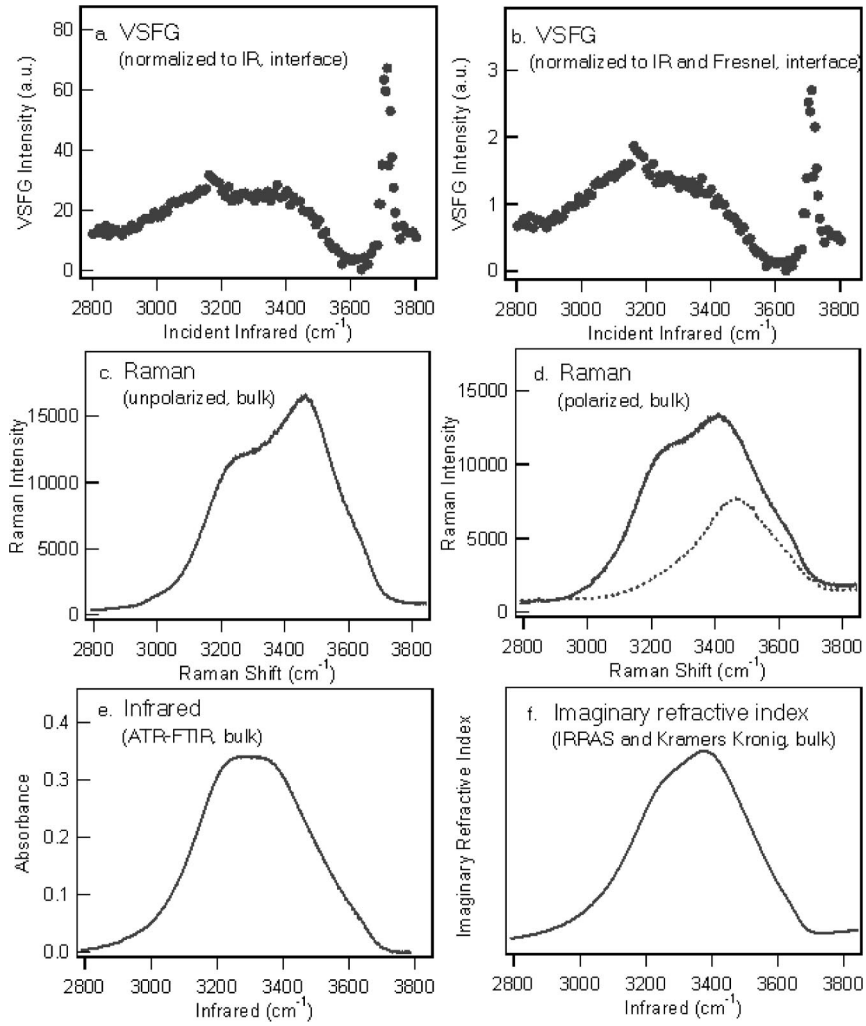

Figure 1. (a) The ssp-polarized VSFG spectrum of the air−water interface with normalization to the real-time IR profile; (b) ssp-polarized VSFG spectrum of the air−water interface with normalization to the real-time IR profile and Fresnel factors; (c) unpolarized Raman spectrum of neat water; (d) parallel (solid line) and perpendicular (dashed line) polarized Raman spectra of neat water; (e) infrared spectrum of neat water obtained from ATR-FTIR; (f) imaginary refractive index of neat water as a function of wavenumber obtained using IRRAS and the Kramers−Kronig transformation.

of 0.056 x. Similar to the unpolarized Raman spectra, there is a decrease in the 3200 cm^{-1} side of the hydrogen-bonded continuum in the parallel-polarized Raman spectra of nitrate salt solutions (Figure 3a). The spectral features of the perpendicular spectra (Figure 3b) show only subtle changes with the addition of nitrate salts. These spectra are consistent with previously reported Raman spectra.[35] For this work, we focus on the unpolarized and the parallel-polarized Raman.

IRRAS experiments were also conducted for nitrate aqueous solutions, and spectra are shown in Figure 4a. Figure 4b,c presents the real (n) and imaginary (k) refractive index spectra extracted from the IRRAS spectra by using the Kramers−Kronig tranformation. Both n and k spectra of neat water obtained through our IRRAS experiments and Kramers−Kronig tranformation are higher than values found in the literature.[36,37] (The refractive index values obtained from the literature rather than from our IRRAS experiments are employed in the determination of Fresnel factors and the normalization of VSFG spectra.) However, n and k spectra of neat water shown in Figure 4b,c follow the same shape as the refractive index spectra obtained by other groups.[36,37] (We are interested in the spectral features rather than the absolute values of n and k, and therefore, the y-axis values of n and k spectra have been removed in Figures 1f and 4b,c.) As shown in Figure 4c, the k spectra of nitrate salt solutions show a decrease of the 3200 cm^{-1} band and no enhancement of the 3400 cm^{-1} band, other than a slight broadening, compared to the neat water, similar to the ATR-FTIR spectra (Figure 2c,d). Moreover, the decrease of the 3200 cm^{-1} band in the k spectra follows the trend water, $Mg(NO_3)_2$, $Ca(NO_3)_2$, and $Sr(NO_3)_2$, which is consistent with the trend observed in the ATR-FTIR spectra. The consistencies between the k spectra and the ATR-FTIR spectra indicate that the IRRAS spectra, as well as the ATR-FTIR and the transmission FTIR spectra, are dominated by the bulk information of the solutions. In this work, we utilize the ATR-FTIR data for the IR bulk spectral data.

The changes in the Raman (Figures 2a,b and 3a) and IR (Figures 2c,d and 4c) spectra of the hydrogen-bonded OH stretch upon the addition of nitrate salts relative to that of neat water are attributed to the water hydrogen-bonding network distortion and the solvation of ions. Due to the presence of metal cations and nitrate anions in aqueous solutions, the displacement of water molecules by these ions results in an intensity loss of the 3200 cm^{-1} band in the Raman and IR spectra. The water molecules that solvate the ions give rise to a small but significant intensity enhancement of the 3400 cm^{-1} band in the Raman spectra. The difference in the Raman and IR spectra is associated with different selection rules.[4]

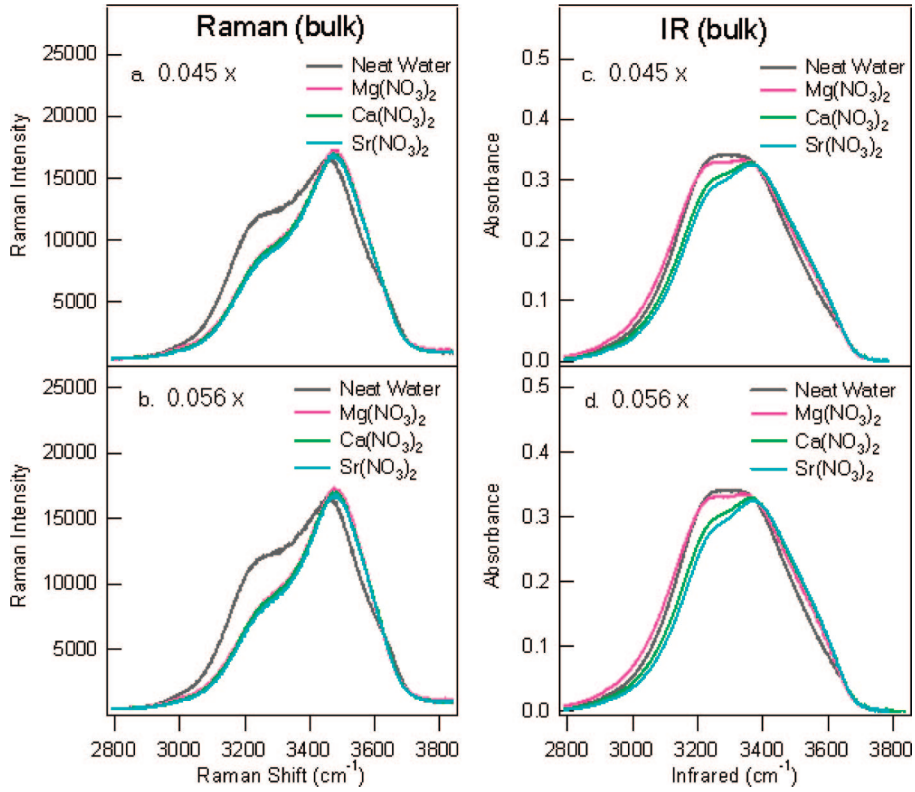

Figure 2. Raman and infrared spectra of aqueous nitrate solutions and neat water: (a) Raman spectra of nitrate solutions with a concentration of 0.045 x (mole fraction); (b) Raman spectra of nitrate solutions with a concentration of 0.056 x; (c) IR spectra of nitrate solutions with a concentration of 0.045 x; (d) IR spectra of nitrate solutions with a concentration of 0.056 x. The spectrum of neat water is plotted in each figure for comparison.

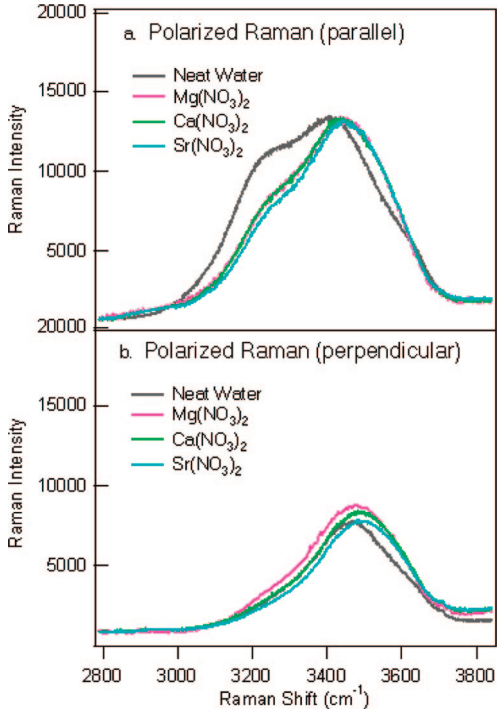

Figure 3. Polarized Raman spectra of 0.056 x nitrate aqueous solutions and neat water: (a) parallel-polarized Raman spectra; (b) perpendicular-polarized Raman spectra.

In previous studies of aqueous sodium halides and hydrogen halides, the Raman intensity enhancement of the 3400 cm^{-1} band has been found to be associated with the size and the polarizability of the anion ($Cl^- < Br^- < I^-$).[4,11] For instance, Br^- has a polarizability approximately twice as high as that of Cl^-, as listed in Table 2. The Raman spectra of NaBr and NaCl aqueous solutions show an intensity enhancement of the 3400 cm^{-1} band for NaBr solutions compared to that for NaCl.[4] The difference is significant especially in more concentrated solutions (0.036 x, which equates to 2.1 m).[4] However, when the size and the polarizability of the metal cation changes, our Raman results show that the intensity of the 3400 cm^{-1} band remains constant. For nitrate salt solutions of $Mg(NO_3)_2$ and $Ca(NO_3)_2$ with concentrations 0.045 and 0.056 x, as shown in Figures 2a,b and 3a, the 3400 cm^{-1} band intensity does not vary with the polarizability of the cation, though Ca^{2+} has a polarizability 10 times as high as that of Mg^{2+} (Table 2). Additional Raman experiments of chloride solutions, $MgCl_2$ and $CaCl_2$, were conducted, and results show that $MgCl_2$ and $CaCl_2$ have the same Raman intensity of the 3400 cm^{-1} band (spectra not shown here). The experiments on chlorides further reveal that the Raman intensity is not sensitive to the polarizability of the cation. It is highly likely that the anion solvation effects rather than the cation solvation effects are the dominant factor that influences the 3400 cm^{-1} band intensity.

Interestingly, Raman results of $NaNO_3$, NaCl, and NaBr aqueous solutions reveal different effects from the nitrate anions on the 3400 cm^{-1} Raman intensity compared to those for the halide anions. (Spectra are shown in the Supporting Information.) As listed in Table 2, nitrate has a polarizability of 27, which is between the polarizability values of Cl^- (19) and Br^- (30). One might expect that for the solutions with the same concentration, the 3400 cm^{-1} band intensity of $NaNO_3$ would be between the intensities of NaCl and NaBr solutions. However, our Raman spectra show that the 3400 cm^{-1} band intensity follows the trend water < $NaNO_3$ < NaCl < NaBr, which does not follow the same trend as the polarizability. The structure of

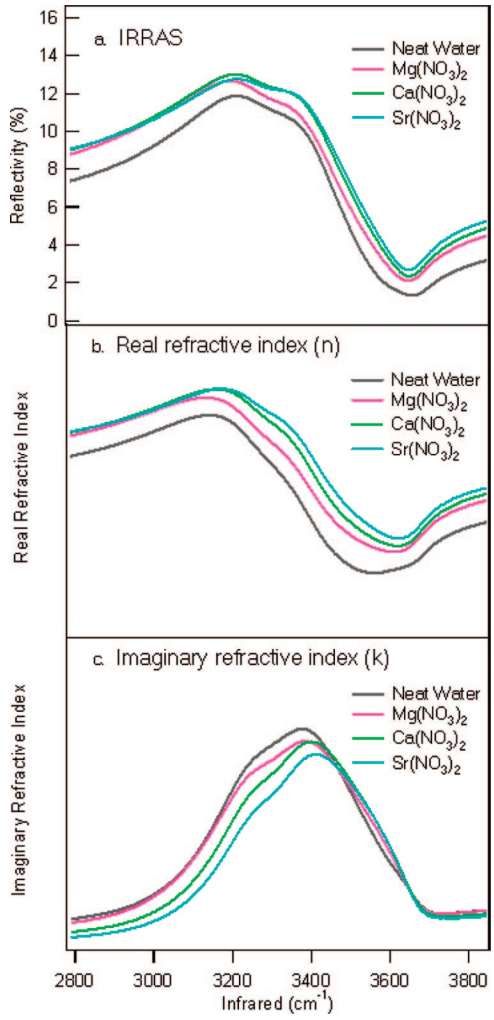

Figure 4. (a) IRRAS spectra of 0.056 x nitrate aqueous solutions and neat water; (b) real refractive indices obtained through Kramers−Kronig transformation of IRRAS spectra; (c) imaginary refractive indices obtained through Kramers−Kronig transformation of IRRAS spectra.

TABLE 2: Polarizability Values of Cations and Anions (Sr^{2+} and I^- Polarizabilities Did Not Converge)

Polarizabilities (bohr^3)	B3PW91/6-311++G(2df,2p)
Be^{2+}	0.045
Mg^{2+}	0.317
Ca^{2+}	3.191
Sr^{2+}	
F^-	5.157
Cl^-	18.783
Br^-	30.994
I^-	
NO_3^-	27.231

nitrate may account for the inconsistency between the Raman intensity and the anion polarizability. Halides, Cl^- and Br^-, are considered spherical in aqueous solutions, whereas nitrate has a planar structure, though distortion may occur due to the interaction with water molecules and cations. The anion structure difference affects the hydration solvation structure.

The VSFG spectra of aqueous $Mg(NO_3)_2$, $Ca(NO_3)_2$, and $Sr(NO_3)_2$ solutions with the same concentrations as those used in the Raman and IR studies are presented in Figure 5. The VSFG spectrum of neat water is plotted for comparison. All VSFG spectra in Figure 5 were normalized to IR intensities only. Though small differences of the VSFG spectra are observed after further normalization to the Fresnel factors, the spectral changes of nitrate aqueous solutions relative to those of neat water remain similar for the two normalization methods, normalization to IR only versus normalization to IR and the Fresnel factors. In the calculation of Fresnel factors, the refractive index of the interface was estimated using the Lorentz slab model (see Supporting Information). (The VSFG spectra of nitrate aqueous solutions with different normalization methods are shown in the Supporting Information.)

Two polarization combinations for the VSFG spectra, ssp and ppp, were obtained. The ssp- and ppp-polarized VSFG spectra that were normalized to IR intensities are shown in Figure 5a−c and d−f, respectively. Upon the addition of nitrate salts, the ssp-polarized VSFG spectra (Figure 5a−c) show a depletion in the 3200 cm^{-1} band, an intensity enhancement in the 3400 cm^{-1} band, and an intensity decrease in the 3700 cm^{-1} peak relative to neat water. The enhancement of the 3400 cm^{-1} band amplifies as the cation of the nitrate salt varies from Mg^{2+} to Ca^{2+} to Sr^{2+}. Additional VSFG experiments of lower-concentration (0.0089 x) $Mg(NO_3)_2$ (the inset of Figure 3a) show that the spectral changes become more significant with increasing concentration. In the ppp-polarized VSFG spectra (Figure 5d−f), however, no intensity decrease of the 3700 cm^{-1} peak is observed for the nitrate aqueous solutions compared to that of neat water.

The VSFG spectra provide structural information at the air−aqueous interface. Recall that VSFG transition moments are related to Raman and IR transition moments;[28,30,34] therefore, it is not surprising to observe an intensity decrease of the 3200 cm^{-1} band in the VSFG spectra of the nitrate solutions relative to that of neat water. Yet, the 3200 cm^{-1} intensity loss in the VSFG spectra is much greater than that in the Raman and IR spectra (Figures 2 and 3).

Shultz and co-workers proposed the presence of contact ion pairs in the surface zone of salt solutions that would neutralize the electric double layer and therefore diminish the 3200 cm^{-1} band.[7] In the case of $Ca(NO_3)_2$ and $Sr(NO_3)_2$ solutions, the formation of contact ion pairs between the metal cation and the interfacial nitrate anion is possible and may contribute to the intensity loss of the 3200 cm^{-1} band of the VSFG spectra shown in Figure 5b,c and e,f. In the case of $Mg(NO_3)_2$, as suggested by the VSFG study of the symmetric stretching modes of nitrate,[25] the presence of solvent-separated and solvent-shared ion pairs is possible. The observed depletion of the 3200 cm^{-1} band of our VSFG spectra shown in Figure 5a−f is likely due to the displacement of interfacial water molecules by ions and relevant ion pairs.

The intensity loss of the 3200 cm^{-1} band in the VSFG spectra is correlated with the increase of the 3400 cm^{-1} band, as shown in Figure 5a−f. This intensity increase of the 3400 cm^{-1} band is attributed to water molecules solvating the ions and ion pairs, disrupting the hydrogen-bonding network at the air−aqueous interface. Although, if we think about this with respect to a shift in population, the VSFG spectrum is sampling the solvation shell of the ions (3400 cm^{-1} band). Since there are six to seven water molecules per ion in these experiments, all of these water molecules are involved in ion solvation.

To further explore the effects of nitrate salts on water structure at the air−aqueous interface and in the bulk, curve fitting analysis was completed. Figure 6 shows the ssp-polarized VSFG intensities of the 3400 cm^{-1} band (the somewhat centrosymmetric solvation shell) from the 0.056 x nitrate aqueous solutions and neat water. The parallel-polarized Raman × IR intensities are also plotted for comparison with the VSFG intensities. Recall

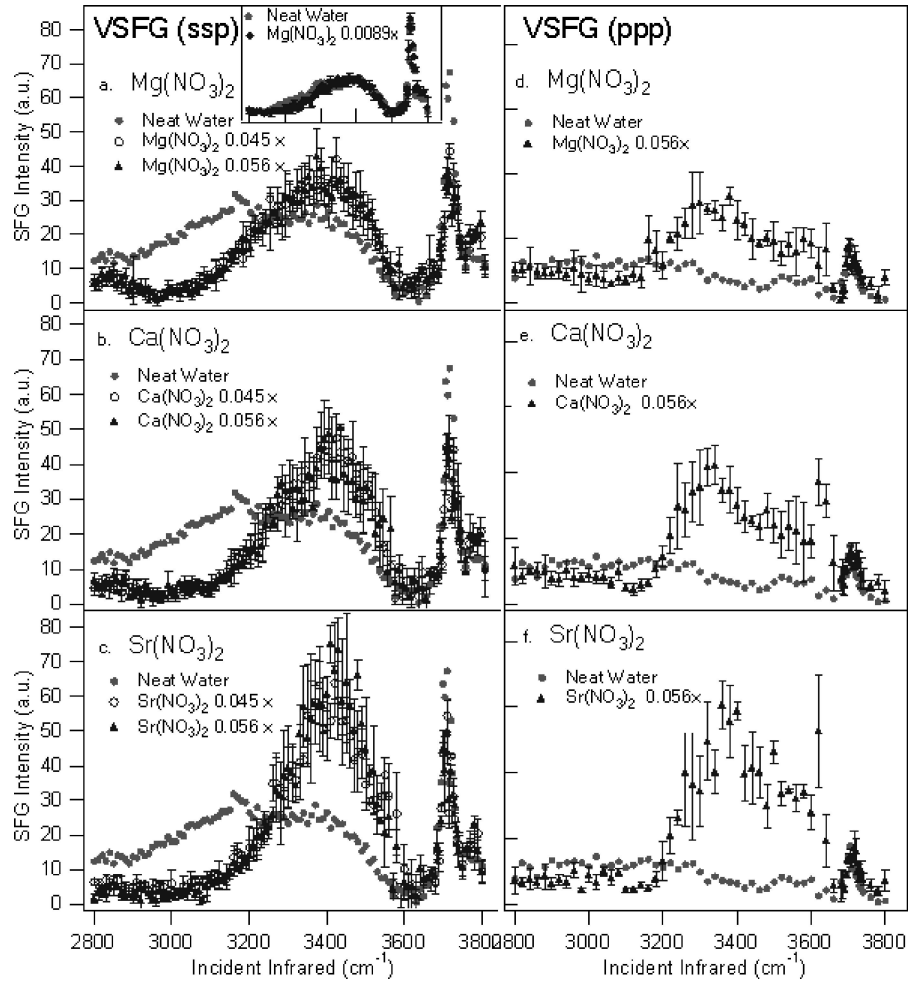

Figure 5. (a) The ssp-polarized VSFG spectra of 0.045 and 0.056 x $Mg(NO_3)_2$; (b) ssp-polarized VSFG spectra of 0.045 and 0.056 x $Ca(NO_3)_2$; (c) ssp-polarized VSFG spectra of 0.045 and 0.056 x $Sr(NO_3)_2$; (d) ppp-polarized VSFG spectrum of 0.056 x $Mg(NO_3)_2$; (e) ppp-polarized VSFG spectrum of 0.056 x $Ca(NO_3)_2$; (f) ppp-polarized VSFG spectrum of 0.056 x $Sr(NO_3)_2$. Inset of (a) ssp-polarized spectrum of 0.0089 x $Mg(NO_3)_2$. The neat water VSFG spectrum is plotted in each figure for comparison.

that the VSFG intensity of a single vibrational mode (I^{ν}_{VSFG}) is related to the interfacial number density (N) squared and the Raman and IR transition moments (α_{lm} and μ_n, respectively) by the equation[38] below

$$I^{\nu}_{\mathrm{VSFG}} \propto N^2\left(\sum_{lmn}\langle\mu_{IJK:lmn}\rangle\langle g|\alpha_{lm}|\nu\rangle\langle\nu|\mu_n|g\rangle\right)^2$$

where $\mu_{IJK:lmn}$ represents the Euler angle transformation between the laboratory coordinates (I, J, K) and the molecular coordinates (l, m, n) and $\langle ... \rangle$ represents an average over the orientational distribution of the interfacial molecules. Therefore, if it were possible to obtain a Raman and IR spectrum of the same exact volume within the interface as the VSFG experiments with the same polarization properties, multiplying the Raman times the IR intensity would then provide a valid comparison to the VSFG spectrum after interference effects were deconvolved. This is currently not technologically possible. However, in this work, we use the Raman and IR spectra as valid bulk probes. Mathematically, the spectral component band multiplication of the Raman times the IR provides a comparison of the bulk to the interface. (We utilize parallel-polarized Raman because the VSFG is ssp-polarized, where the ss combination is mathematically comparable to the parallel Raman process.) Thus, to clarify differences between the bulk and the interface, the bulk Raman × IR intensities of the 3400 cm^{-1} bands are compared after normalization with water to the interfacial VSFG intensities of

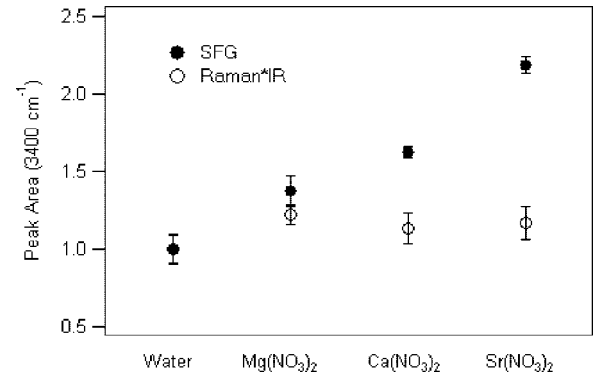

Figure 6. Integrated peak areas of the 3400 cm^{-1} solvation band for ssp-polarized VSFG and Raman × IR (parallel-polarized Raman area multiplied by IR area) to compare the water number density of the air−aqueous interface to the bulk. (The VSFG intensity is proportional to the square of the number density.) Areas were normalized to neat water for 0.056 x aqueous solutions.

the 3400 cm^{-1} component band, as shown in Figure 6. Component bands are used for the comparison to alleviate the effects of interference since VSFG is a coherent spectroscopy. Additionally, of importance is the fact that VSFG is sensitive to the orientation of water molecules. According to recent phase-sensitive VSFG studies of air−water interfaces,[39] the imaginary part of the second-order susceptibility, Im $\chi^{(2)}$, at 3400 cm^{-1} is

negative, indicating that these water molecules have an average stretch dipole moment pointing toward the liquid. Yet, with ions present in the solution, the 3400 cm^{-1} band is attributed to water molecules solvating the ions and ion pairs. Due to the centrosymmetric character of solvation shells, the stretch dipoles of water molecules cancel each other out to some extent. Additionally, the nitrate anions that approach the air−aqueous interface and the cations that reside deeper in the solution may create a static field. This induced static field may reorient part of the interfacial water molecules toward the vapor phase and produce a third-order signal. The second and third contributions are not independently resolvable currently. If only considering the second-order susceptibility contribution, we expect a less negative or smaller absolute value of the Im $\chi^{(2)}$ at 3400 cm^{-1} due to the reorientation of water molecules caused by the presence of the static field. This is consistent with the results from phase studies.[39] Yet, it is important to remember that the 3400 cm^{-1} region is probing semicentrosymmetric solvation structures, and therefore, in the analysis below, we can only predict a lower limit on the number of water molecules and thus a lower limit of the increase in interfacial depth.

Compared to the Raman and IR spectra, the VSFG intensity increase of the 3400 cm^{-1} band with the addition of nitrate salts is more significant. This is clear from the spectra (Figures 2−5) and from the fitting results from the component bands (Figure 6). The 3400 cm^{-1} band intensity differences between different nitrate solutions are unique at the interface.

An increase in interfacial depth would increase the number of molecules probed by VSFG and thus the intensity of VSFG. This is what is observed and shown in Figure 6. In VSFG studies, the interface is defined by the concentration gradient of different species and lack of an inversion center; the bulk begins where the concentrations are homogeneously mixed, and there is macroscopic inversion symmetry.[4,38] Thus, an increase in interfacial depth accounts for the VSFG intensity differences of the 3400 cm^{-1} component band of all of the nitrate solutions studied here.

To understand the differences in the 3400 cm^{-1} component band of the VSFG spectra, the band areas from the different divalent cation nitrate solutions are compared. From Figure 5 and the subsequent fitting results from the 3400 cm^{-1} band plotted in Figure 6, the VSFG intensity enhancement of the 3400 cm^{-1} band amplifies with the size of the cation ($Mg^{2+} < Ca^{2+} < Sr^{2+}$) for nitrate solutions. This is inconsistent with the Raman and IR spectra. Nitrate anions in the air−aqueous interfacial region attract the metal cations toward the interface. At the same time, the cations also impose a bulk driving force on the nitrate anions at the interface, according to Newton's Third Law.[13] On the basis of our recent VSFG study of nitrate aqueous interfaces,[25] for cations with relatively large size and low surface charge density, for instance, Sr^{2+} and Ca^{2+}, the metal−nitrate ion pairing (the interaction between metal cations and interfacial nitrate anions) is enhanced relative to that for Mg^{2+}. Therefore, we expect that the water solvation of ions and ion pairs also varies with cation identity. The ion pairing and the water solvation account for the distribution inhomogeneity of ions in the interfacial region, and different metal cations have different effects. It is likely that for nitrate solutions with large size of the divalent metal cations, the interface probed by VSFG extends deeper into the solution. In other words, the concentration gradient extends over a larger region for $Sr(NO_3)_2$ and $Ca(NO_3)_2$ solutions relative to that for $Mg(NO_3)_2$. The relative change in concentration gradient explains the observed 3400 cm^{-1} band enhancement in the VSFG spectra, which follows the trend $Mg(NO_3)_2 < Ca(NO_3)_2 < Sr(NO_3)_2$.

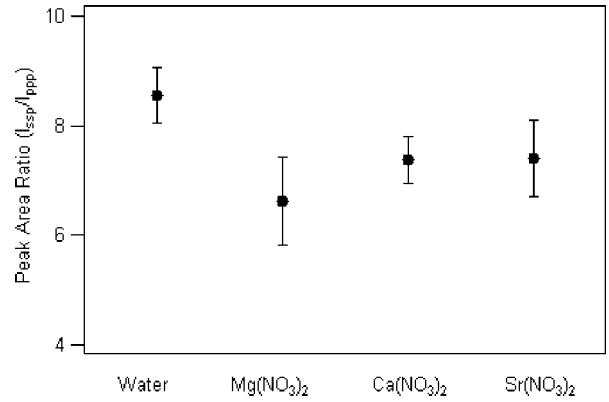

Figure 7. Free OH peak area ratio of the ssp- to the ppp-polarized VSFG for neat water and 0.056 x nitrate aqueous solutions.

The ssp-polarized VSFG spectra of the nitrate salt solutions reveal an intensity decrease in the 3700 cm^{-1} free OH peak relative to that of neat water, as shown in Figure 5a−c. An intensity decrease could be from a free OH population decrease, an orientation change, or both. Although clearly resolved in our spectra and shown in the VSFG sodium nitrate studies completed by the Shultz group,[7] the intensity decrease in the 3700 cm^{-1} peak is not observed in other VSFG studies of lower-concentration aqueous inorganic salt solutions.[4,6,7,38] Such an intensity decrease is observed for acid solutions however.[11] The interfacial water structure was proposed to undergo a structural reorganization upon the addition of acid, resulting in a decrease of the number of OH bonds projecting into the air.[11] According to our pH measurements, the pH of $Ca(NO_3)_2$ and $Sr(NO_3)_2$ solutions is close to that of nanopure water, while $Mg(NO_3)_2$ solutions are slightly more acidic. Relative to previous air−aqueous acid interfacial studies,[11] the pH of nitrate salt solutions is not significantly impacting the free OH intensity.

Unlike the ssp-polarized VSFG spectra, in the ppp-polarized VSFG spectra (Figure 5d−f), no intensity change of the 3700 cm^{-1} free OH peak is observed for the nitrate aqueous solutions relative to neat water. Figure 7 shows the free OH intensity ratio of the ssp- to the ppp-polarized VSFG (I_{ssp}/I_{ppp}). For neat water, the I_{ssp}/I_{ppp} ratio is around 8.5, which is similar to the values obtained from other groups.[40,41] For nitrate aqueous solutions, the I_{ssp}/I_{ppp} ratio decreases to 6.6−7.3 (Figure 7), indicating an orientation change of the free OH at the air−aqueous nitrate interface. Using previously calculated $C_{\infty v}$ orientation data,[40] the free OH of the nitrate solutions is determined to be tilted from the surface normal. There are two solutions to the obtained I_{ssp}/I_{ppp} ratio, one being a tilt of angle of ∼30° and the other being a tilt angle of ∼60°. However, the ppp-polarized VSFG free OH intensities of the nitrate aqueous solutions are the same as that in neat water, and therefore, the orientation angle of free OH is determined to be ∼60° from the surface normal.

Conclusions

The water structure at the air−aqueous interface of a series of divalent metal nitrate solutions at relatively high concentrations (0.045 and 0.056 x) was investigated using vibrational sum frequency generation spectroscopy in the OH stretching region of liquid water. Raman (polarized) and infrared spectroscopies were employed to compare the effects of ions on the water structure of the bulk solution to that of the interface.

IRRAS spectra were also analyzed to further understand the VSFG data. The ssp-polarized sum frequency spectra reveal a significant depletion of the strong hydrogen-bonded water OH stretch, an intensity enhancement of the water OH stretch in the relatively weak hydrogen-bonding region, and an intensity decrease of the free OH peak upon the addition of nitrate salts to neat water. These VSFG spectral changes indicate that these ions, and possibly their respective ion pairs, approach the aqueous surface. The interfacial water hydrogen-bonding network is profoundly disturbed as the divalent cation size increases (and as the cation surface charge density decreases). From our previous studies, nitrate was shown to approach the interface, as revealed from direct observation of the nitrate symmetric stretch by VSFG.[25] Here, we observe a combined effect of the nitrate with the divalent countercation. The polarizability of the divalent cations is extremely small when compared to that of nitrate and, more relevant, when compared to that of the halide anions, Br^- and I^-, which previously have been shown to also significantly perturb interfacial water.[4] Therefore, cation polarizabilities are not believed to be solely responsible for this phenomenon. Although the cause (cation size, surface charge density, and/or polarizability) is not clear, the VSFG spectra and our analysis of the contributing Raman and infrared transition-moment strengths indicate that the divalent cations create differing concentration gradients near the surface, thereby increasing the VSFG-active region. Thus, the interface becomes thickened as one moves down the alkali earth group, $Mg^{2+} < Ca^{2+} < Sr^{2+}$. It is critical to note that our comparison of the SFG 3400 cm^{-1} component peak to the Raman and infrared is valid since this spectral region is characterized by solvation shells of the ions, and therefore, the SFG intensity is not enhanced by water alignment from any Coulombic field. Instead, the SFG is undercounting the water molecules in this spectral region due to centrosymmetry of the solvation structures.

Also interesting is the significant change in the free OH orientation at the surface of these solutions. Clearly, the surface of these solutions allows the free OH to continue to exist but significantly alters its orientation from 33° from neat water to ~60° from the surface normal. Surprisingly, this organization does not result in a complete loss of the free OH species since it would seem that the hydrogen of the free OH would be close to a surface oxygen from a surface water molecule. Yet, these salt solutions lack water molecules beyond the first and/or second solvation shell of the ions. That is, the solvating water molecules are interacting with the ions, and one might think that they may not be as available for the free OH to bind to their oxygen as a hydrogen-bonding site. Thus, this observation, continued existence of the free OH, also provides evidence for the surface presence of nitrate anions.

Acknowledgment. We gratefully acknowledge funding of this work from the Department of Energy (DOE-BES, DE-FG02-04ER15495).

Supporting Information Available: Calculations of Fresnel factors, details of VSFG spectra normalization, VSFG spectra of nitrate aqueous solutions with different normalization methods, and Raman spectra of $NaNO_3$, NaCl, and NaBr aqueous solutions. This material is available free of charge via the Internet at http://pubs.acs.org.

References and Notes

(1) Eisenthal, K. B. *Acc. Chem. Res.* **1993**, *26*, 636–643.
(2) Du, Q.; Superfine, R.; Freysz, E.; Shen, Y. R. *Phys. Rev. Lett.* **1993**, *70*, 2313–2316.
(3) Shen, Y. R.; Ostroverkhov, V. *Chem. Rev.* **2006**, *106*, 1140–1154.
(4) Liu, D.; Ma, G.; Levering, L. M.; Allen, H. C. *J. Phys. Chem. B* **2004**, *108*, 2252–2260.
(5) Gopalakrishnan, S.; Liu, D.; Allen, H. C.; Kuo, M.; Shultz, M. J. *Chem. Rev.* **2006**, *106*, 1155–1175.
(6) Raymond, E. A.; Richmond, G. L. *J. Phys. Chem. B* **2004**, *108*, 5051–5059.
(7) Schnitzer, C. S.; Baldelli, S.; Shultz, M. J. *J. Phys. Chem. B* **2000**, *104*, 585–590.
(8) Shultz, M. J.; Baldelli, S.; Schnitzer, C.; Simonelli, D. *J. Phys. Chem. B* **2002**, *106*, 5313–5324.
(9) Durand-Vidal, S.; Simonin, J. P.; Turq, P. *Electrolytes at Interfaces*; Kluwer Academic: Dordrecht, The Netherlands, 2000.
(10) Adamson, A. W.; Gast, A. P. *Physical Chemistry of Surfaces*; Wiley: New York, 1997.
(11) Levering, L. M.; Sierra-Hernandez, M. R.; Allen, H. C. *J. Phys. Chem. C* **2007**, *111*, 8814–8826.
(12) Mucha, M.; Frigato, T.; Levering, L. M.; Allen, H. C.; Tobias, D. J.; Dang, L. X.; Jungwirth, P. *J. Phys. Chem. B* **2005**, *109*, 7617–7623.
(13) Petersen, P. B.; Saykally, R. J. *J. Phys. Chem. B* **2005**, *109*, 7976–7980.
(14) Petersen, P. B.; Saykally, R. J.; Mucha, M.; Jungwirth, P. *J. Phys. Chem. B* **2005**, *109*, 10915–10921.
(15) Ghosal, S.; Hemminger, J. C.; Bluhm, H.; Mun, B. S.; Hebenstreit, E. L. D.; Ketteler, G.; Ogletree, D. F.; Requejo, F. G.; Salmeron, M. *Science* **2005**, *307*, 563–566.
(16) Yang, X.; Kiran, B.; Wang, X. B.; Wang, L. S.; Mucha, M.; Jungwirth, P. *J. Phys. Chem. A* **2004**, *108*, 7820–7826.
(17) Jungwirth, P.; Tobias, D. J. *Chem. Rev.* **2006**, *106*, 1259–1281.
(18) Jungwirth, P.; Tobias, D. J. *J. Phys. Chem. B* **2001**, *105*, 10468–10472.
(19) Jungwirth, P.; Tobias, D. J. *J. Phys. Chem. B* **2002**, *106*, 6361–6373.
(20) Dang, L. X.; Chang, T. M. *J. Phys. Chem. B* **2002**, *106*, 235–238.
(21) Salvador, P.; Curtis, J. E.; Tobias, D. J.; Jungwirth, P. *Phys. Chem. Chem. Phys.* **2003**, *5*, 3752–3757.
(22) Minofar, B.; Vacha, R.; Wahab, A.; Mahiuddin, S.; Kunz, W.; Jungwirth, P. *J. Phys. Chem. B* **2006**, *2006*, 15939–15944.
(23) Thomas, J. L.; Roeselova, M.; Dang, L. X.; Tobias, D. J. *J. Phys. Chem. A* **2007**, *111*, 3091–3098.
(24) Dang, L. X.; Chang, T. M.; Roeselova, M.; Garrett, B. C.; Tobias, D. J. *J. Chem. Phys.* **2006**, *124*, 066101.
(25) Xu, M.; Tang, C. Y.; Jubb, A.; Chen, X.; Allen, H. C. *J. Phys. Chem. C* **2009**, *113*, 2082.
(26) Sovago, M.; Wurpel, G.; Smits, M.; Muller, M.; Bonn, M. *J. Am. Chem. Soc.* **2007**, *129*, 11079–11084.
(27) Shen, Y. R. *The Principle of Nonlinear Optics*, 1st ed.; John Wiley & Sons: New York, 1984.
(28) Lambert, A. G.; Davies, P. B. *Appl. Spectrosc. Rev.* **2005**, *40*, 103–145.
(29) Xu, M.; Larentzos, J. P.; Roshdy, M.; Criscenti, L. J.; Allen, H. C. *Phys. Chem. Chem. Phys.* **2008**, *10*, 4793–4801.
(30) Zhuang, X.; Miranda, P. B.; Kim, D.; Shen, Y. R. *Phys. Rev. B* **1999**, *59*, 12632–12640.
(31) Richmond, G. L. *Chem. Rev.* **2002**, *102*, 2693–2724.
(32) Smith, J. D.; Cappa, C. D.; Wilson, K. R.; Cohen, R. C.; Geissler, P. L.; Saykally, R. J. *Proc. Natl. Acad. Sci. U.S.A.* **2005**, *102*, 14171–14174.
(33) Wang, Z.; Pang, Y.; Dlott, D. D. *J. Phys. Chem. A* **2007**, *111*, 3196–3208.
(34) Wang, H.-F.; Gan, W.; Lu, R.; Rao, Y.; Wu, B.-H. *Int. Rev. Phys. Chem.* **2005**, *24*, 191–256.
(35) Levering, L. M. *A Vibrational Spectroscopic Study of Aqueous Hydrogen Halide Solutions: Application to Atmospheric Aerosol*; Chemistry,The Ohio State University: Columbus, OH, 2005.
(36) Bertie, J. E.; Lan, Z. *Appl. Spectrosc.* **1996**, *50*, 1047–1057.
(37) Kocak, A.; Berets, S. L.; Milosevic, V.; Milosevic, M. *Appl. Spectrosc.* **2006**, *60*, 1004–1007.
(38) Gopalakrishnan, S.; Jungwirth, P.; Tobias, D. J.; Allen, H. C. *J. Phys. Chem. B* **2005**, *109*, 8861–8872.
(39) Ji, N.; Ostroverkhov, V.; Tian, C. S.; Shen, Y. R. *Phys. Rev. Lett.* **2008**, *100*, 096102.
(40) Gan, W.; Wu, D.; Zhang, Z.; Guo, Y.; Wang, H.-F. *Chin. J. Chem. Phys.* **2006**, *19*, 20–24.
(41) Wei, X.; Shen, Y. R. *Phys. Rev. Lett.* **2001**, *86*, 4799–4802.

JP806565A